ANTIMICROBIAL AGENTS AND CHEMOTHERAPY, Oct. 2006, p. 3435–3443 Vol. 50, No. 10
0066-4804/06/$08.00+0 doi:10.1128/AAC.00386-06


# Structure-Activity Relationships of *Bacillus cereus* and *Bacillus anthracis* Dihydrofolate Reductase: toward the Identification of New Potent Drug Leads

Tammy M. Joska[1] and Amy C. Anderson[2]*

*Department of Biochemistry, Dartmouth Medical School, Hanover, New Hampshire 03755,[1] and Department of Pharmaceutical Science, University of Connecticut, Storrs, Connecticut 06269[2]*

Received 29 March 2006/Returned for modification 9 May 2006/Accepted 30 June 2006

**New and improved therapeutics are needed for *Bacillus anthracis*, the etiological agent of anthrax. To date, antimicrobial agents have not been developed against the well-validated target dihydrofolate reductase (DHFR). In order to address whether DHFR inhibitors could have potential use as clinical agents against *Bacillus*, 27 compounds were screened against this enzyme from *Bacillus cereus*, which is identical to the enzyme from *B. anthracis* at the active site. Several 2,4-diamino-5-deazapteridine compounds exhibit submicromolar 50% inhibitory concentrations ($IC_{50}$s). Four of the inhibitors displaying potency in vitro were tested in vivo and showed a marked growth inhibition of *B. cereus*; the most potent of these has $MIC_{50}$ and minimum bactericidal concentrations at which 50% are killed of 1.6 μg/ml and 0.09 μg/ml, respectively. In order to illustrate structure-activity relationships for the classes of inhibitors tested, each of the 27 inhibitors was docked into homology models of the *B. cereus* and *B. anthracis* DHFR proteins, allowing the development of a rationale for the inhibition profiles. A combination of favorable interactions with the diaminopyrimidine and substituted phenyl rings explains the low $IC_{50}$ values of potent inhibitors; steric interactions explain higher $IC_{50}$ values. These experiments show that DHFR is a reasonable antimicrobial target for *Bacillus anthracis* and that there is a class of inhibitors that possess sufficient potency and antibacterial activity to suggest further development.**

Although known for years to cause sporadic life-threatening disease, *Bacillus anthracis*, the etiological agent of anthrax, has recently attracted attention as a potential bioterrorism weapon. The highly virulent nature of anthrax necessitates that prophylactic treatment with antibiotics be started prior to the presentation of symptoms to have the greatest efficacy. While fluoroquinolones and cephalosporins are currently recommended for the treatment of anthrax, these treatments have serious limitations, including the lack of indication for children and the development of resistance (2, 6, 8).

Dihydrofolate reductase (DHFR) has been a widely recognized antimicrobial drug target as it plays a key role in the generation of the DNA base dTMP. Specifically, DHFR catalyzes the reduction of dihydrofolate, using NADPH to form tetrahydrofolate and $NADP^+$. *B. anthracis* exhibits a natural resistance to trimethoprim (TMP), a clinically used antibacterial DHFR inhibitor, due to a lack of affinity between the enzyme and the inhibitor (2). In fact, most reported cases of DHFR insensitivity to antibiotics stem from changes of residues at the active site. For example, mutations of active-site residues also occur in strains of *Plasmodium falciparum* resistant to pyrimethamine and cycloguanil (23). Trimethoprim resistance reported to occur in bacteria, including *Streptococcus pneumoniae* (1, 12) and *Staphylococcus aureus* (7), also involves amino acid substitutions. In both cases, although other mutations may modulate the degree of resistance, active-site mutations of Ile100Leu and Phe98Tyr, respectively, were necessary for resistance. At positions homologous to these two residues, *Bacillus cereus* and *B. anthracis* DHFRs ($DHFR_{Bc}$ and $DHFR_{Ba}$, respectively) contain phenylalanine, explaining the natural resistance of the *Bacillus* enzymes to TMP.

In spite of the resistance to TMP, other classes of DHFR inhibitors may inhibit the enzyme with sufficient potency to have potential use as clinical agents. In this report, we present data that show 98% sequence identity between the DHFR proteins of *B. cereus* and *B. anthracis*, allowing both proteins to be evaluated as drug targets. *B. anthracis* and *B. cereus* are closely related genetically (15) but exhibit different phenotypes after infection; infection with *B. cereus*, usually as a food contaminant, causes endophthalmitis, bacteremia, septicemia, endocarditis, pneumonia, and meningitis (10). The *B. cereus* DHFR protein was cloned, expressed, and purified. Twenty-seven inhibitors were tested using an in vitro enzyme assay; four inhibitors were tested in antibacterial assays, and all of these showed growth inhibition of *B. cereus*. Two inhibitors with the lowest 50% inhibitory concentrations ($IC_{50}$s), other than methotrexate, showed $MIC_{50}$ values of 1.6 and 2.6 μg/ml and minimal bactericidal concentrations at which 50% of strains are killed ($MBC_{50}$s) of 0.09 and 1.4 μg/ml against the *B. cereus* strain. Finally, we built homology models of the *B. cereus* and *B. anthracis* DHFR proteins, docked all of the tested inhibitors, and developed a structure-activity relationship (SAR) that explains the enzyme inhibition results. These results show that antifolates are capable of inhibiting the *Bacillus* DHFR enzyme as well as inhibiting the growth of *Bacillus* in culture.

* Corresponding author. Mailing address: Department of Pharmaceutical Science, 69 N. Eagleville Rd., University of Connecticut, Storrs, CT 06269. Phone: (860) 486-6145. Fax: (860) 486-6857. E-mail: Amy.Anderson@uconn.edu.

## MATERIALS AND METHODS

**Materials.** All materials used were reagent grade, unless otherwise stated. The substrate, DHF, was a gift from Eprova (Switzerland). β-NADPH was purchased from Sigma and resuspended in sterile water for enzyme assays. Methotrexate (compound 1), trimethoprim (compound 19), and pyrimethamine (compound 24) were purchased from Sigma and resuspended in a 50% dimethyl sulfoxide (DMSO) solution for enzyme assays. Twenty-six inhibitors were kindly provided by the Rosowsky laboratory (Dana-Farber Cancer Institute, Boston, MA), and one inhibitor (compound 18) was provided by the Gangjee laboratory (Duquesne University). These inhibitors were resuspended in a DMSO and sterile water solution at various concentrations. The synthesis and preparation of the inhibitors have been described previously for compounds 2 and 10 (17), 3 (20), 4 to 9 (18), 11 to 16 (19), 17 (16), 18 (9), 20 and 22 (18), 21 and 23 (17), and 25 to 27 (21) (see Fig. 3 to 5 for compounds of groups 1 to 3).

**Sequence homology analysis and alignment.** The *B. anthracis* DHFR protein was used as a probe in a BLAST search to find the closest bacterial sequences and structural homologs. Protein sequence information for the following organisms was gathered from the Protein Data Bank at the National Center for Biotechnology Information (NCBI): *B. cereus*, accession number AAP09158; *B. anthracis*, accession number AAT40581; *Escherichia coli*, accession number AAN78554; and *Homo sapiens*, accession number NP00782. T-Coffee (13) was used to perform the primary sequence alignment.

**Cloning.** The sequence for the *B. cereus* DHFR gene was PCR amplified (LA *Taq* polymerase; Takara) from genomic DNA (ATCC 14579) obtained from the *Bacillus* Genomic Stock Center (Department of Biochemistry, The Ohio State University) with primers from Integrated DNA Technologies (IDT). The gene included 486 nucleotides and encoded a protein of 162 amino acids. The forward primer 5′-GCTCATATGATTGTTTCATTTATGGTCGCTATG-3′ and reverse primer 5′-GCACTCGAGTTGTCGCTTCTCATATACATGATAATA-3′ were used under standard PCR conditions, with an annealing temperature of 50°C. The gene was inserted into the pET41 vector (Novagen) to include a six-His tag at the C terminus for nickel affinity column purification. The expression plasmid was created by digesting the vector and insert with the restriction endonucleases NdeI and XhoI (New England Biolabs), followed by ligation with T4 DNA ligase. Competent DH5α cells (Invitrogen) were transformed, and a circularized-plasmid-containing insert was recovered and sequenced to ensure that no errors were generated in the PCR. Competent BL21(DE3) cells (Novagen) were transformed with purified plasmid for recombinant protein expression.

**Recombinant protein overexpression and purification.** BL21(DE3) transformants were grown in Luria broth (LB) containing 30 μg/ml kanamycin at 37°C with shaking at 250 rpm to mid-logarithmic-phase growth, and expression was induced by the addition of isopropyl-β-D-thiogalactopyranoside (IPTG) to a final concentration of 1 mM. Recombinant protein expression was extended for 6 h at 37°C. Expressed cells were harvested by centrifugation at 10,000 × *g* for 10 min and placed at −80°C until cell lysis occurred. To harvest proteins, the cell pellet from 1 liter of induced cells was resuspended in 15 ml of Bug Buster (Novagen) for chemical lysis. The cell suspension was placed on an orbital shaker for 20 min at room temperature in the presence of 2 mM phenylmethylsulfonyl fluoride (PMSF). The cell extract was centrifuged at 50,000 × *g* for 20 min, and the clarified supernatant was passed through a 0.45-μm filter (Millipore) before it was loaded onto a 6-ml nickel affinity column (Fast Flow nickel resin; QIAGEN) for single-step purification to homogeneity. The column was preequilibrated with buffer (50 mM Tris [pH 7.0], 50 mM KCl) and eluted using a 0 to 250 mM imidazole gradient over 10 column volumes after being washed with 5 column volumes of the equilibration buffer. Fractions containing purified DHFR, as determined by sodium dodecyl sulfate-polyacrylamide gel electrophoresis (SDS-PAGE) analysis with silver staining, were pooled and exchanged into a buffer containing 50 mM Tris-HCl (pH 7.0), 50 mM KCl, 0.5 mM EDTA, and 10 mM dithiothreitol. Protein was frozen using an ethanol-dry ice bath and stored at −80°C.

**In vitro inhibition assays.** Enzyme activity assays were performed at 25°C by monitoring the rate of enzyme-dependent NADPH consumption at an absorbance of 340 nm over a period of several minutes. Reactions were performed in the presence of 20 mM TES [*N*-tris(hydroxymethyl)methyl-2-aminoethanesulfonic acid; pH 7.0], 50 mM KCl, 10 mM 2-mercaptoethanol, 0.5 mM EDTA, and 1 mg/ml bovine serum albumin. Saturating cofactor and substrate concentrations (100 μM NADPH and 1 mM DHF, respectively) were used in the presence of a limiting concentration of enzyme. After an incubation period of 5 min in the presence or absence of the inhibitor, the reaction was initiated with the addition of dihydrofolate. The reactions were performed a minimum of four times to determine the average rate and 50% inhibitory concentration values with standard deviations in the presence of various concentrations of inhibitor near the $IC_{50}$.

**Antibacterial assays.** Spores (*Bacillus* Genetic Stock Center) were added to a petri dish of LB agar in the absence of antibiotic selection in a sterile environment. Three drops of LB were added to rehydrate the spores. The plate was streaked with a sterile tip, and a second plate was streaked from the first and placed in a 37°C incubator overnight. A third plate was streaked to isolate single colonies. A culture (50 ml) was inoculated from the single colony and grown overnight at 37°C with shaking at 225 rpm.

The optical density at 600 nm ($OD_{600}$) of the log-phase culture was estimated from the $OD_{600}$ of the stationary-phase growth. A 1:100 dilution of an overnight culture was grown until the $OD_{600}$ reached 1.0, and the numbers of CFU were determined by plating 100 μl of $10^{-2}$, $10^{-4}$, and $10^{-6}$ dilutions of the log-phase culture. The numbers of CFU determined for cultures at an $OD_{600}$ of 1.0 were used to estimate appropriate dilutions for plating test cultures in the presence and absence of the inhibitor.

To monitor cell growth in the presence and absence of the inhibitor, methods described previously were used as guides (24). A 1:100 dilution of an overnight culture at stationary-phase growth was grown until the $OD_{600}$ reached 1.0. From the mid-logarithmic-phase culture, $6 \times 10^5$ cells were added to 1-ml test cultures in the presence or absence of an antibiotic ranging in concentration from 0.11 to 21.1 μg/ml. Cultures were grown for 9 hours, and the $OD_{600}$ was monitored during that period to determine $MIC_{50}$ values for each inhibitor tested. For control cultures, the corresponding volume of DMSO was added.

The numbers of CFU were determined by adjusting the cultures from the growth inhibition assay to an $OD_{600}$ of 1.0 and then diluting the cultures further to $10^{-4}$, $10^{-5}$, and $10^{-6}$ cells/ml. One hundred microliters from each dilution was plated on an LB agar plate and incubated overnight at 37°C. Single colonies were counted from the respective plates, and the numbers of CFU/ml of cells were calculated.

**Homology modeling.** Using the 3D-JIGSAW (3) server and an automated approach, homology models of $DHFR_{Bc}$ and $DHFR_{Ba}$ were determined based on the structure of *E. coli* DHFR, the closest known homolog. Both homology models were superimposed to detect any differences. Since there was no significant difference between the models, one model was minimized with SYBYL (Tripos, Inc.). Methotrexate (MTX) bound to $DHFR_{Bc}$ was modeled using FlexE (Tripos, Inc.). Briefly, ensembles of the protein active site were prepared by molecular dynamic runs using a radius of 2.5 Å around the ligand bound in the active site for 1,000 fs. The inhibitor, MTX, was docked to the ensemble with an incremental ligand construction and scored using the empirical scoring function available in FlexE. The modeled enzyme-bound MTX was brought into XtalView to analyze the SARs of the inhibitors. Briefly, the inhibitors were individually minimized using SYBYL. The 2,4-diaminopyrimidine ring common to each inhibitor was superimposed on the diaminopyrimidine ring of MTX, and the remainder of the structure was manipulated through any rotatable bonds to place the conserved derivatized phenyl group in the hydrophobic pocket.

## RESULTS

**Sequence comparisons.** $DHFR_{Bc}$ is used as a model for $DHFR_{Ba}$ since the two proteins are 98% identical (Fig. 1a). Both species of DHFR include a 486-nucleotide open reading frame that encodes a 162-residue protein. Only three residues, Val77Ala, Ile130Met, and Ile138Val, all of which are peripheral to the binding pocket, differ between the species (Fig. 1b). Val77Ala and Ile138Val occur on separate β strands and are involved in hydrophobic packing between strands. Ile130Met is located within a relatively unstructured loop region on the protein.

**Protein analysis.** The purified $DHFR_{Bc}$ fusion protein included two extra residues (L and E) at the C terminus, which resulted from inclusion of the restriction site XhoI, followed by a six-His tag for nickel affinity column chromatography. The resulting fusion protein consists of 170 residues with an approximate size of 20 kDa. The average specific activity of the $DHFR_{Bc}$ protein is 11.1 ± 1.9 units/mg ($n = 9$), which is comparable to the specific activities of other species of DHFRs

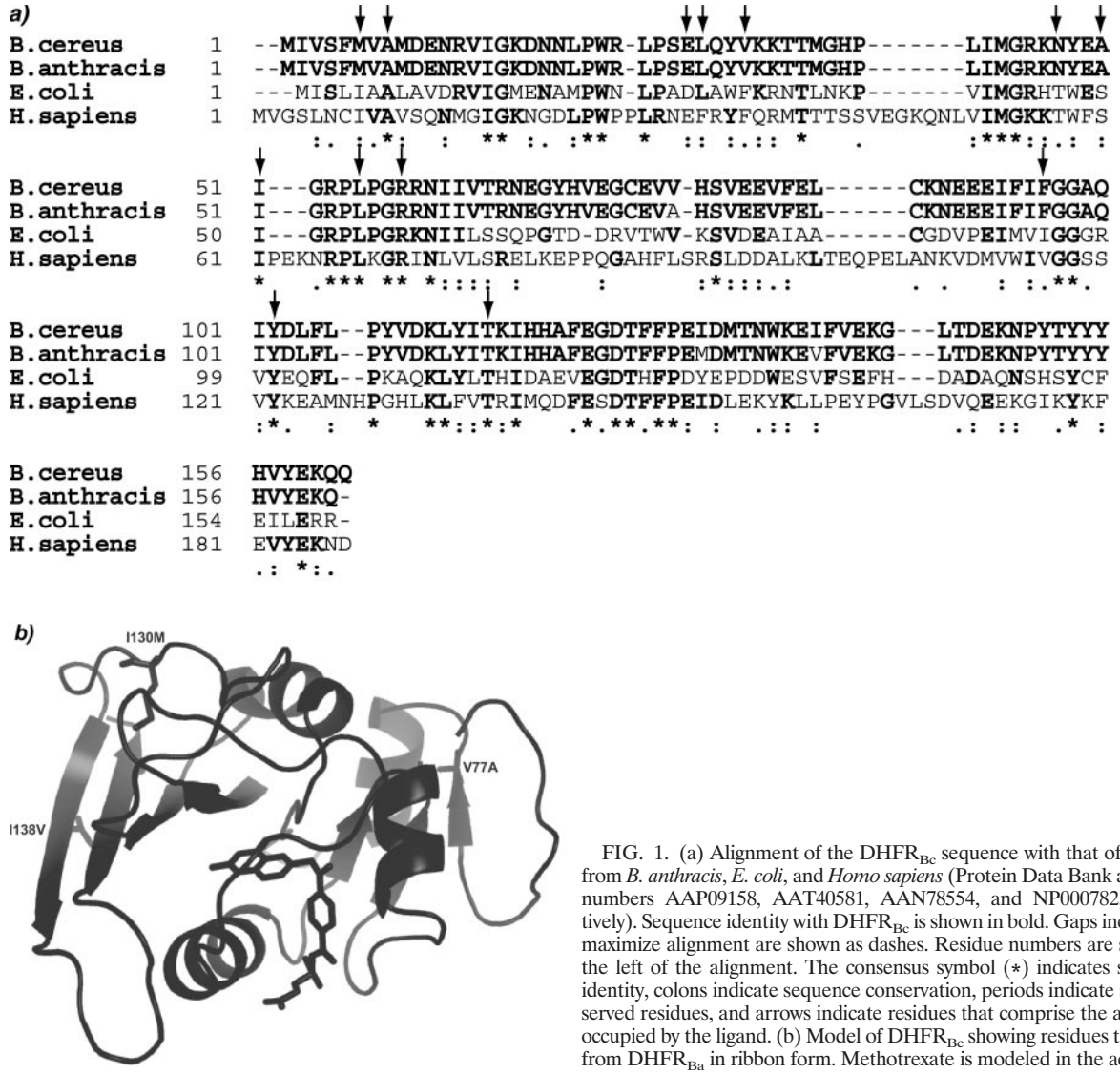


FIG. 1. (a) Alignment of the $DHFR_{Bc}$ sequence with that of DHFRs from *B. anthracis*, *E. coli*, and *Homo sapiens* (Protein Data Bank accession numbers AAP09158, AAT40581, AAN78554, and NP000782, respectively). Sequence identity with $DHFR_{Bc}$ is shown in bold. Gaps included to maximize alignment are shown as dashes. Residue numbers are shown to the left of the alignment. The consensus symbol (*) indicates sequence identity, colons indicate sequence conservation, periods indicate semiconserved residues, and arrows indicate residues that comprise the active site occupied by the ligand. (b) Model of $DHFR_{Bc}$ showing residues that differ from $DHFR_{Ba}$ in ribbon form. Methotrexate is modeled in the active site.

(11, 22, 25). Purification produced a total of ~150 mg of expressed protein per liter of cells. Protein was determined to be soluble at concentrations in excess of 25 mg/ml. $DHFR_{Bc}$ is a single polypeptide as determined by both SDS-PAGE (Fig. 2) and native gel electrophoresis.

**Evaluation of enzyme inhibitors.** In order to obtain SAR information for these species, 27 inhibitors were screened for binding $DHFR_{Bc}$ using a standard spectrophotometric enzyme assay. All of the inhibitors include a 2,4-diaminopyrimidine scaffold, which is believed to compete with dihydrofolate to bind a conserved glutamic acid residue (Glu 28 for $DHFR_{Bc}$) in the active site. The enzyme inhibitor assays were repeated at least four times to give $IC_{50}$ values with standard deviations. The screened inhibitors exhibited a broad range of $IC_{50}$ values between 24 nM and greater than 1 mM (Table 1).

The inhibitors are divided into three groups, based on their structural class. Group 1 contains pteridines, 5-deazapteridines, a quinazoline, and a pyrrolopyrimidine (Fig. 3). Compound 1 (MTX) is highly potent ($IC_{50}$ = 24 nM), but other pteridine compounds (compounds 11 to 17) display $IC_{50}$ values that range from 2.2 to >1,000 μM. The single quinazoline (compound 3) yields an $IC_{50}$ value of 1.1 μM, but the 5′-deazapteridines (compounds 2 and 4 to 10) yielded $IC_{50}$ values ranging from 0.27 to 1.9 μM; and four of these compounds (2, 6, 7, and 8) were selected for in vivo testing. Interestingly, compound 16, which is very similar in structure to compound 15, binds weakly and has an $IC_{50}$ value that far exceeds 100 μM. This decrease in $IC_{50}$ value is attributed to the presence of the methyl group extending from the diaminopteridine ring.

The second group of inhibitors (compounds 19 to 24) represents pyrimidine derivatives with $IC_{50}$ values between 37 and >1,000 μM. Both TMP (compound 19) and pyrimethamine (compound 24) are included in this group (Fig. 4). The third group of inhibitors, representing complex diaminonaphthoquinazoline derivatives (compounds 25 to 27), showed no inhibition of $DHFR_{Bc}$, even at concentrations greater than 1 mM (Fig. 5).

Enzyme-inhibitor assays with clinically used DHFR inhibi-

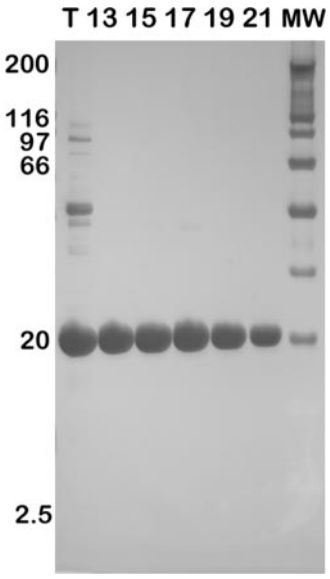


FIG. 2. Twelve percent SDS-PAGE showing the purification of recombinant $DHFR_{Bc}$. Lane T, cell extract from BL21(DE3) cells transformed with $DHFR_{Bc}$ expression plasmids; lanes 13 to 21, fractions from the nickel affinity chromatography column; MW, molecular weight markers (molecular weights are indicated at the left in thousands). The bottom edge of the gel is indicative of the dye front.

tors such as methotrexate (compound 1), trimethoprim (compound 19), and pyrimethamine (compound 24) show $IC_{50}$ values of 24 nM, 43 μM, and greater than 100 mM, respectively. The values for methotrexate and trimethoprim in this study compare well, within experimental error, with those reported by Barrow et al. (2) for *Bacillus anthracis* Sterne DHFR (12.2 ± 3 nM and 77.3 ± 20 μM, respectively), further emphasizing the similarity of $DHFR_{Bc}$ and $DHFR_{Ba}$.

**Antibacterial assays.** Four of the most potent compounds (2, 6, 7, and 8) were tested in standard growth inhibition assays and were found to inhibit the growth of *B. cereus* in culture. The values for the $MIC_{50}$ and $MIC_{90}$ relative to those for control cultures were determined experimentally (Table 2). Bacterial growth was monitored by recording the optical densities at 600 nm prior to the addition of antibiotic and every hour for up to 10 h after the addition of antibiotic to capture the lag, log, and stationary phases of growth in the presence and absence of the inhibitor (Fig. 6a and b show these curves for compounds 2 and 8). The compounds are sensitive to light and temperature and appear to degrade after overnight incubation at 37°C; therefore, cultures were covered with aluminum foil to minimize light exposure, and incubation times did not exceed 10 h.

The MBCs required to kill 50 and 90% of the bacterial strains were also determined for all four compounds (Table 2; Fig. 6c and d depict data for compounds 2 and 8). Cultures that were grown as described above were plated in order to determine the numbers of CFU that survived in the test cultures relative to those in the control cultures. Compound 8 is the most bactericidal, as determined by the $MBC_{50}$ and $MBC_{90}$ values of 0.09 μg/ml and 3.8 μg/ml, respectively.

A number of necrotic cells appeared in the cultures with higher concentrations of inhibitor. These cells most likely contribute to the overall turbidity of the culture but are incapable of forming colonies on agar plates, explaining the lower $MBC_{50}$ values relative to the $MIC_{50}$ values shown in Table 2. The $MBC_{90}$ values in all of these experiments are ≤2.5 times the $MIC_{50}$ values, as has been noted in detailed studies investigating the accuracy of MBC determinations (24) and in numerous studies of *Staphylococcus aureus* (14) and pneumococci (26).

**Homology modeling results.** Since there is no structural information for $DHFR_{Bc}$ or $DHFR_{Ba}$, we created homology models of both $DHFR_{Ba}$ and $DHFR_{Bc}$ based on the structure of an Asp 27-to-Glu 27 mutation of the well-characterized *E. coli* DHFR (Protein Data Bank no. 1DRA) (4) using the program 3D-JIGSAW (3). *E. coli* DHFR was chosen as a parent structure because it has 39% overall identity with $DHFR_{Bc}$ and 61.5% sequence identity (the remaining residues are considered similar) within the active site. Ramachandran plots of the homology models show that 99.4% of the residues fell within acceptable ranges. Ile 93, which is peripheral to the active site, has backbone angles that fall outside the allowed regions. Minimization of the two models independently did not yield any conformational differences, and the two models were superimposed with no apparent structural differences, allowing for the modeling results to pertain to both species. All compounds were modeled in the active site, and interactions with the active-site residues were assessed to interpret the results of the in vitro enzyme assays.

Methotrexate (compound 1) was docked into the active site

TABLE 1. $IC_{50}$ values for inhibitor compounds

| Group | Compound | Mean $IC_{50}$ ± SD[b] |
|---|---|---|
| 1 | 1 (MTX) | 0.024 ± 0.021 |
| | 2[a] | 0.27 ± 0.10 |
| | 3 | 1.1 ± 0.34 |
| | 4 | 0.60 ± 0.11 |
| | 5 | 1.67 ± 0.98 |
| | 6[a] | 0.51 ± 0.51 |
| | 7[a] | 0.88 ± 0.13 |
| | 8[a] | 0.35 ± 0.035 |
| | 9 | 1.85 ± 0.29 |
| | 10 | 1.90 ± 1.36 |
| | 11 | 4.82 ± 1.16 |
| | 12 | 6.32 ± 5.29 |
| | 13 | 2.26 ± 1.73 |
| | 14 | 7.58 ± 1.70 |
| | 15 | 17.61 ± 0.78 |
| | 16 | >1 mM |
| | 17 | 16.67 ± 0.33 |
| | 18 | 252.2 ± 19.2 |
| 2 | 19 (TMP) | 42.96 ± 9.20 |
| | 20 | 37.33 ± 2.58 |
| | 21 | 69.29 ± 24.4 |
| | 22 | 73.73 ± 13.1 |
| | 23 | 150.23 ± 13.1 |
| | 24 (PYR[c]) | >1 mM |
| 3 | 25 | >1 mM |
| | 26 | >1 mM |
| | 27 | >1 mM |

[a] Inhibitor tested in vivo.
[b] $IC_{50}$ values are expressed in μM unless otherwise noted.
[c] PYR, pyrimethamine.

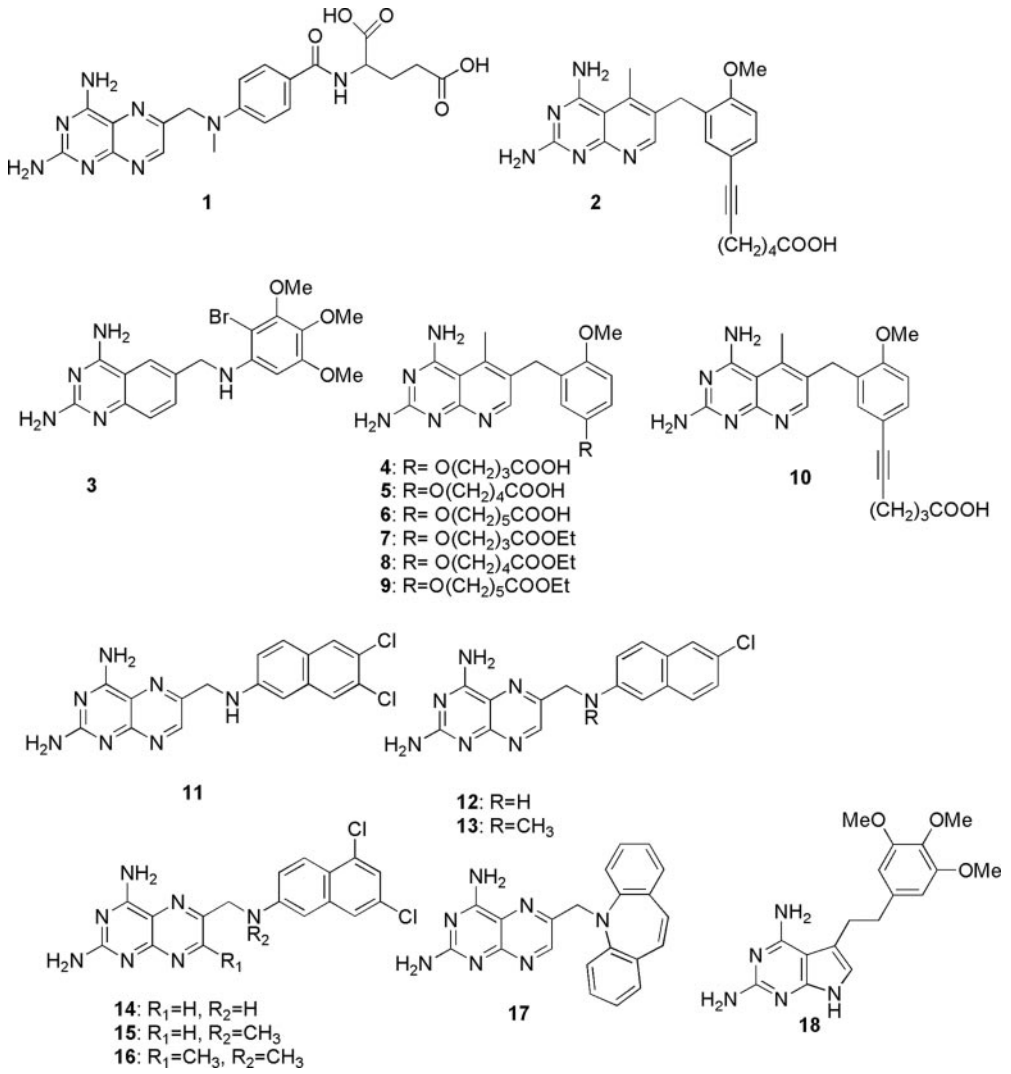


FIG. 3. Group 1 compounds, including pteridines, 5-deazapteridines, a quinazoline, and a pyrrolopyrimidine, tested as $DHFR_{Bc}$ enzyme inhibitors.

using FlexE (5) and an ensemble of molecular dynamic snapshots to simulate a flexible protein model (Fig. 7a). The protonated N-1 and the amino group at position 2 of the diaminopyrimidine ring appear to form the expected hydrogen bonds with Glu 28; other hydrogen bonds are apparent between Tyr 102 and the carbonyl of Met 6. Additional van der Waals interactions are formed between the pteridine ring and Met 6, Phe 96, Ala 8, and Thr 115. The bridge region forms van der Waals interactions with Asn 47, which may also form a hydrogen bond with the carbonyl of Phe 96 and aid in the

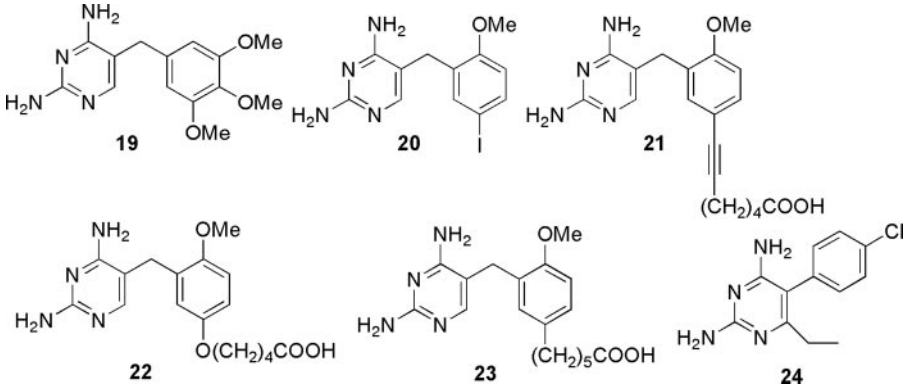


FIG. 4. Group 2 diaminopyrimidine compounds tested as $DHFR_{Bc}$ enzyme inhibitors.

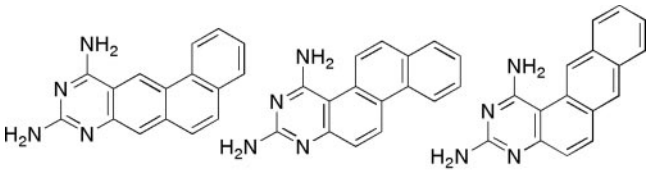


FIG. 5. Group 3 compounds, including the complex diaminonaphthoquinazoline, tested as $DHFR_{Bc}$ enzyme inhibitors.

proper positioning of Phe 96 in the active site. The phenyl ring fits nicely in a hydrophobic pocket comprised of Ile 51, Leu 55, Leu 29, and Val 32. Arg 58 forms hydrogen bonds with one carboxylic acid group, whereas the second appears to extend into solvent.

**Interactions between inhibitors and residues in the active site.** Aside from methotrexate, compounds 2 to 10 have the lowest $IC_{50}$ values, with compound 2 exhibiting an $IC_{50}$ value of 272 nM. Figure 7b shows a model of compound 2 bound in the active site. The diaminopyrimidine rings in compounds 2 to 10 are expected to form many of the same interactions as the diaminopyrimidine ring of methotrexate, including the same hydrogen bonds and van der Waals interactions. The additional methyl group on the pyridopyrimidine ring appears to make a hydrophobic interaction with Phe 96. The 2′ methoxy group forms van der Waals interactions with a small hydrophobic pocket comprised of Leu 21, Trp 23, and Ile 117. The 5′ methoxy group forms van der Waals interactions with Leu 29 and Val 32. The differences between compounds 2 to 10 reside in the type of chain at the 5′ position and the length of the chain. The alkyl chain generally binds in a hydrophobic environment comprised of Leu 29, Leu 55, and the backbone of Lys 33. Since the alkyl portion of the chain is relatively long (greater than three carbons), either the acetylene (compounds 2 and 10) or ether (compounds 4 to 9) linkage allows the same approximate degree of flexibility for the terminal group of the chain. The terminal group, whether a COOH or a COO ethyl, appears to be capable of forming hydrogen bonds with either Arg 58, Arg 53, or Lys 33. The similarity in the $IC_{50}$ values in this series, despite the differences in the chain types and lengths, most likely reflects the flexibility of the tail as well as arginine side chains in forming this important stabilizing interaction.

The other compounds in group 1 include several pteridines (compounds 11 to 17) and a pyrrolopyrimidine (compound 18). Again, the pteridine rings of these compounds are expected to form the same interactions as the pteridine ring in methotrexate. The two-atom bridge forms van der Waals interactions with Phe 96 and Asn 47. For compounds 11 to 15, the substituted naphthyl rings appear to make hydrophobic interactions with Leu 29, Val 32, Ile 51, and Leu 55. The decrease in the affinity of these inhibitors relative to that of methotrexate could be caused by the loss of the interactions of the glutamate tail, including the salt bridge formed with Arg 58, or the projection of the hydrophobic naphthyl ring into the solvent exterior. The dibenzazepine ring of compound 17 likely forms hydrophobic contacts with Ile 51, Ala 50, Lys 46, and Leu 21 and additionally explores a larger hydrophobic binding pocket defined by Leu 21, Lys 46, Trp 23, and Ile 15, usually left vacant by the standard single-phenyl ring inhibitors.

Pyrimidine inhibitors in group 2 (compounds 19 to 24), illustrated by the model of compound 20 in the active site (Fig. 7c), generally have $IC_{50}$ values between 37 and 73 μM, with the exception of compounds 23 and 24, which have values of 150 and >1,000 μM, respectively. The higher $IC_{50}$ values for compounds 19 to 22, relative to those observed with the pteridines and the 5-deazapteridines are explained by the inability of the single-pyrimidine ring and single-atom bridge to place the phenyl ring in the hydrophobic pocket normally occupied by the *p*-aminobenzoic acid ring of MTX. Pyrimethamine (compound 24), a common antifolate, exhibits very poor binding to $DHFR_{Bc}$. The chlorophenyl group projects directly into the space occupied by Asn 47, causing steric interactions. Additionally, pyrimethamine does not utilize the hydrophobic pocket comprised of Ile 51, Leu 55, Leu 29, and Val 32. However, the ethyl group projecting from position 5 of 2,4-diaminopyrimidine has revealed a further small hydrophobic binding pocket defined by Leu 21 and Trp 23. Trimethoprim (compound 19) forms the canonical interactions between the diaminopyrimidine ring and Glu 28, Tyr 102, Met 6, Ala 8, and Thr 115; however, the trimethoxyphenyl ring does not appear to extend fully into the hydrophobic pocket and may exhibit steric conflict with Asn 47, possibly explaining its lower potency.

The inhibitors that comprise group 3 are generally ineffective due to steric interactions with residues in the binding pocket (Fig. 7d shows compound 23 in the active site). Phe 96 normally forms hydrophobic contacts with the bicyclic ring structure of the diaminopyrimidine rings of the more potent analogs, yet in these inhibitors, there are steric interactions with Phe 96. Asn 47 also appears to form steric interactions with the multiple-ring structures of these inhibitors.

## DISCUSSION

Infections from *Bacillus* organisms, including *B. cereus* and *B. anthracis*, present a threat that could potentially be controlled with prophylactic antibiotics. With the inclusion of *B. anthracis* in the list of category A pathogens, research to find stable and effective antibiotics that can be delivered to a broad population including children has become a greater concern.

In this report, we present data showing the validity of dihydrofolate reductase as a drug target for two different microbes, *B. cereus* and *B. anthracis*, sharing 98% sequence identity for this enzyme. The residue differences are conservative. Purified $DHFR_{Bc}$ was shown to be stable and soluble at high concen-

TABLE 2. MICs and MBCs determined in antibacterial assays[a]

| Compound | $MIC_{50}$ | $MIC_{90}$ | $MBC_{50}$ | $MBC_{90}$ |
|---|---|---|---|---|
| 2 | 2.6 | 10.5 | 1.4 | 3.9 |
| 6 | 11.3 | 21.2 | 5.5 | 12.2 |
| 7 | 3.6 | 11.2 | 1.5 | 7.7 |
| 8 | 1.6 | 4.4 | 0.09 | 3.8 |

[a] Values are expressed in μM.

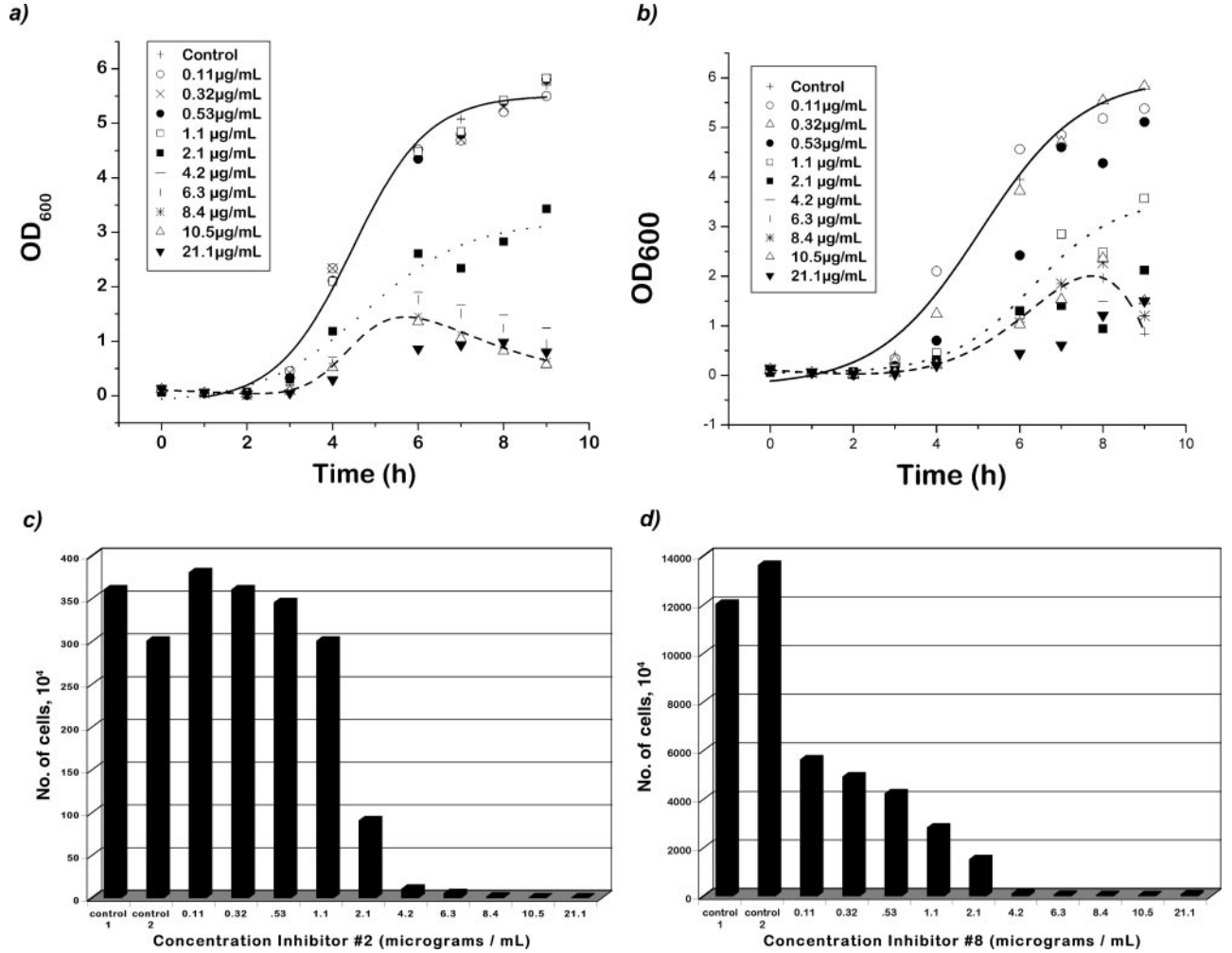


FIG. 6. Growth inhibition of *B. cereus*. Growth curves are shown for control cultures (without the inhibitor present) and for several cultures containing different concentrations of compound 2 (a) and compound 8 (b). Bactericidal concentrations were determined for compound 2 (c) and compound 8 (d).

trations and to have catalytic activity comparable to those of other species of DHFR. Using 27 inhibitors with a 2,4-diaminopyrimidine scaffold, we describe an SAR model supported by structural evidence based on homology models of $DHFR_{Ba}$ and $DHFR_{Bc}$. Four inhibitors that were potent in vitro were also shown to be potent in vivo; two of the most potent inhibitors display growth inhibition with a correspondingly high degree of cell death.

Inhibitory profiles have been developed previously for many of these compounds against *Pneumocystis carinii* ($DHFR_{Pc}$), *Toxoplasma gondii* ($DHFR_{Tg}$), *Mycobacterium avium* ($DHFR_{Ma}$), and rat liver DHFR (rlDHFR). Clearly, methotrexate (compound 1) is a very potent compound, but it possesses a high degree of mammalian cell toxicity and is currently used for the treatment of human cancer; therefore, it is not a viable option for the treatment of anthrax. Compound 2 is potent against $DHFR_{Pc}$, $DHFR_{Tg}$, and $DHFR_{Ma}$ ($IC_{50}$s of 0.87, 0.072, and 0.041 μM, respectively); it is less potent against rat liver DHFR (25 μM), yielding some selectivity (17). Inhibition data for compounds 4 to 6 show that an alkyl tail with four methylene carbons is most potent toward *Bacillus* DHFRs, but for $DHFR_{Ma}$ there was little difference in inhibition among alkyl tails with chain lengths of five to eight carbons (18). Data for compounds 7 to 9 show that an alkyl tail with six methylene carbons is most potent against $DHFR_{Pc}$ and $DHFR_{Tg}$ (18), although the differences in $IC_{50}$ values as the lengths of the alkyl tails varied were smaller. Against $DHFR_{Bc}$, compound 8 (tail length of four carbons) was one of the most potent compounds. Compound 3 is most potent against $DHFR_{Tg}$ ($IC_{50}$ = 0.039 μM); the $IC_{50}$ value for $DHFR_{Bc}$ was similar to that for $DHFR_{Pc}$ and rlDHFR (9). Compound 17, the dibenzazepine, has submicromolar $IC_{50}$ values against all three pathogenic species: $DHFR_{Pc}$, $DHFR_{Tg}$, and $DHFR_{Ma}$. The value for $DHFR_{Bc}$ is closer to that for rlDHFR (4.4 μM) (16). Compound 18 has relatively high $IC_{50}$ values for all species, including $DHFR_{Bc}$ but with the exception of $DHFR_{Tg}$ ($IC_{50}$ = 8.1 μM) (9). Compounds 21 to 23 have submicromolar $IC_{50}$ values for $DHFR_{Pc}$, $DHFR_{Tg}$, and $DHFR_{Ma}$; the values for rat liver and $DHFR_{Bc}$ are higher (17, 18). This profile is expected, since compounds 21 to 23 are TMP analogs and the $IC_{50}$ for TMP against

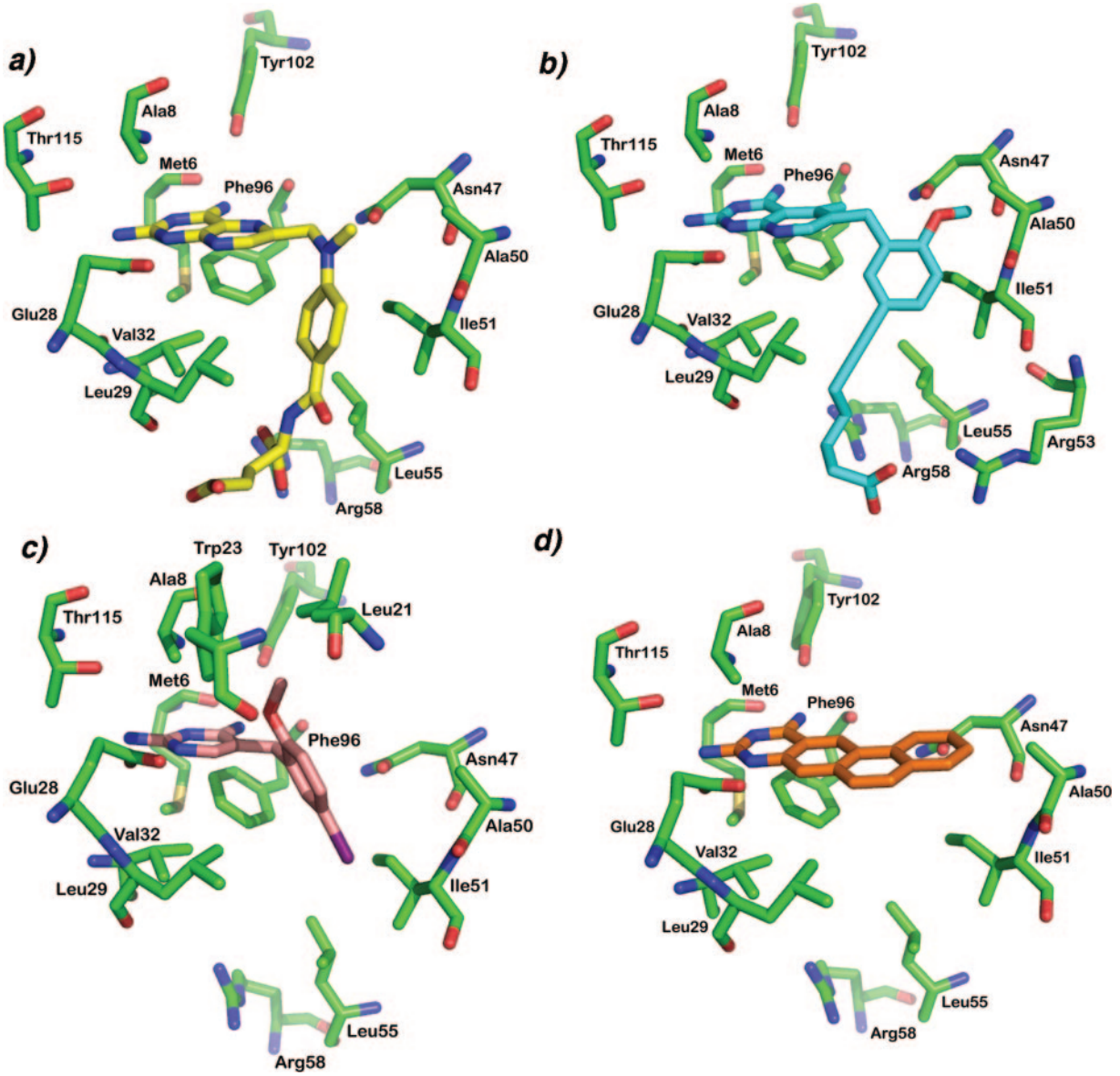


FIG. 7. Models of several DHFR inhibitors interacting with residues in the active site. (a) Methotrexate (compound 1) (yellow); (b) compound 2 (cyan); (c) compound 20 (salmon); (d) compound 23 (orange). (b, c, and d) Characteristic group 1, 2, and 3 inhibitors, respectively.

$DHFR_{Bc}$ is much higher than those for these other species.

These studies have shown that a class of DHFR inhibitors is capable of inhibiting the enzyme with sufficient efficiency to suggest further development of DHFR inhibitors for potential clinical use against *B. cereus* and *B. anthracis*. The inhibitors tested in these studies are potent, but specificity must also be incorporated in an effective inhibitor. Interestingly, compound 2 exhibits low activity ($IC_{50}$ = 25 μM) against rat liver DHFR (17) and exhibits submicromolar affinity for $DHFR_{Bc}$, suggesting that it may be a good lead for further development for increased potency and selectivity. Among the residues which strictly comprise the $DHFR_{Ba}$ or $DHFR_{Bc}$ active site and are intimately involved in substrate binding, there are several key differences that can be exploited in the development of specific inhibitors. Met 6 in $DHFR_{Bc}$ is replaced by an isoleucine in the human form of DHFR, Asn 47 is replaced by a Thr, and Ala 50 is replaced by a serine in the human form. Two phenylalanine residues in human DHFR (Phe 31 and Phe 34) are replaced by smaller hydrophobic residues (Leu 29 and Val 32, respectively). These residues may be critical to the development of potent antimicrobials specific for $DHFR_{Bc}$ or $DHFR_{Ba}$. In addition, structural information will be valuable for further insight into the development of new inhibitors.

## ACKNOWLEDGMENTS

This work was supported by NIGMS grant GM67542.

We thank Andre Rosowsky and Aleem Gangjee for providing inhibitors and James Throckmorton for assistance with initial FlexE docking runs.

## REFERENCES


1. **Adrian, P. V., and K. P. Klugman.** 1997. Mutations in the dihydrofolate reductase gene of trimethoprim-resistant isolates of *Streptococcus pneumoniae*. Antimicrob. Agents Chemother. **41:**2406–2413.
2. **Barrow, E. W., P. C. Bourne, and W. W. Barrow.** 2004. Functional cloning of *Bacillus anthracis* dihydrofolate reductase and confirmation of natural resistance to trimethoprim. Antimicrob. Agents Chemother. **48:**4643–4649.
3. **Bates, P., L. Kelley, R. MacCallum, and M. Sternberg.** 2001. Enhancement of protein modeling by human intervention in applying the automatic programs 3D-JIGSAW and 3D-PSSM. Proteins **45:**39–46.
4. **Bystroff, C., and J. Kraut.** 1991. Crystal structure of unliganded *Escherichia coli* dihydrofolate reductase. Ligand-induced conformational changes and cooperativity in binding. Biochemistry **30:**2227–2239.
5. **Claussen, H., C. Buning, M. Rarey, and T. Lengauer.** 2001. FlexE: efficient molecular docking considering protein structure variations. J. Mol. Biol. **308:**377–395.
6. **Coker, P. R., K. L. Smith, and M. E. Hugh-Jones.** 2002. Antimicrobial susceptibilities of diverse *Bacillus anthracis* isolates. Antimicrob. Agents Chemother. **46:**3843–3845.
7. **Dale, G., C. Broger, A. D'Arcy, P. Hartman, R. DeHoogt, S. Jolidon, I. Kompis, A. Labhardt, H. Langen, H. Locher, M. Page, D. Stuber, R. Then, B. Wipf, and C. Oefner.** 1997. A single amino acid substitution in *Staphylococcus aureus* dihydrofolate reductase determines trimethoprim resistance. J. Mol. Biol. **266:**23–30.
8. **Davidson, R., R. Cavalcanti, J. Brunton, D. Bast, J. DeAzavedo, P. Kibsey, C. Fleming, and D. Low.** 2002. Resistance to levofloxacin and failure of treatment of pneumococcal pneumonia. N. Engl. J. Med. **346:**747–750.
9. **Gangjee, A., F. Mavandadi, S. Queener, and J. McGuire.** 1995. Novel 2,4-diamino-5-substituted-pyrrolo[2,3-d]pyrimidines as classical and nonclassical antifolate inhibitors of dihydrofolate reductases. J. Med. Chem. **38:**2158–2165.
10. **Hoffmaster, A., J. Ravel, D. Rasko, G. Chapman, M. Chute, C. Marston, B. De, C. Sacchi, C. Fitzgerald, L. Mayer, M. Maiden, F. Priest, M. Barker, L. Jiang, R. Cer, J. Rilstone, S. Peterson, R. Weyant, D. Galloway, T. Read, T. Popovic, and C. Fraser.** 2004. Identification of anthrax toxin genes in a *Bacillus cereus* associated with an illness resembling inhalation anthrax. Proc. Natl. Acad. Sci. USA **101:**8449–8454.
11. **Leartsakulpanich, U., M. Imwong, S. Pukrittayakamee, N. White, G. Snounou, W. Sirawaraporn, and Y. Yuthavong.** 2002. Molecular characterization of dihydrofolate reductase in relation to antifolate resistance in *Plasmodium vivax*. Mol. Biochem. Parasitol. **119:**63–73.
12. **Maskell, J. P., A. M. Sefton, and L. M. C. Hall.** 2001. Multiple mutations modulate the function of dihydrofolate reductase in trimethoprim-resistant *Streptococcus pneumoniae*. Antimicrob. Agents Chemother. **45:**1104–1108.
13. **Notredame, C., D. Higgins, and J. Heringa.** 2000. T-Coffee: a novel method for multiple sequence alignments. J. Mol. Biol. **302:**205–217.
14. **Pelletier, L. L., and C. B. Baker.** 1988. Oxacillin, cephalothin, and vancomycin tube macrodilution MBC result reproducibility and equivalence to MIC results for methicillin-susceptible and reputedly tolerant *Staphylococcus aureus* isolates. Antimicrob. Agents Chemother. **32:**374–377.
15. **Radnedge, L., P. G. Agron, K. K. Hill, P. J. Jackson, L. O. Ticknor, P. Keim, and G. L. Andersen.** 2003. Genome differences that distinguish *Bacillus anthracis* from *Bacillus cereus* and *Bacillus thuringiensis*. Appl. Environ. Microbiol. **69:**2755–2764.
16. **Rosowsky, A., V. Cody, N. Galitsky, H. Fu, A. Papoulis, and S. Queener.** 1999. Structure-based design of selective inhibitors of dihydrofolate reductase: synthesis and antiparasitic activity of 2,4-diaminopteridine analogues with a bridged diarylamine side chain. J. Med. Chem. **42:**4853–4860.
17. **Rosowsky, A., R. Forsch, and S. Queener.** 2003. Further studies on 2,4-diamino-5-(2′,5′-disubstituted benzyl)pyrimidines as potent and selective inhibitors of dihydrofolate reductases from three major opportunistic pathogens of AIDS. J. Med. Chem. **46:**1726–1736.
18. **Rosowsky, A., R. Forsch, and S. Queener.** 2002. Inhibition of *Pneumocystis carinii*, *Toxoplasma gondii* and *Mycobacterium avium* dihydrofolate reductases by 2,4-diamino-5-[2-methoxy-5-(ω-carboxyalkoxy)benzyl]pyrimidines: marked improvement in potency relative to trimethoprim and species selectivity relative to piritrexim. J. Med. Chem. **45:**233–241.
19. **Rosowsky, A., R. Forsch, S. Queener, and J. Bertino.** 1997. Synthesis of 2,4-diaminopteridines with bulky lipophilic groups at the 6-position as inhibitors of *Pneumocystis carinii*, *Toxoplasma gondii* and mammalian dihydrofolate reductase. Pteridines **8:**173–187.
20. **Rosowsky, A., C. Mota, and S. Queener.** 1996. Brominated trimetrexate analogues as inhibitors of *Pneumocystis carinii* and *Toxoplasma gondii* dihydrofolate reductase. J. Heterocycl. Chem. **33:**1959–1966.
21. **Rosowsky, A., and N. Papathanasopoulos.** 1974. Quinazolines. XIII. Synthesis of polycyclic 2,4-diaminopyrimidines from aromatic amine hydrochlorides and sodium dicyanamide. J. Org. Chem. **39:**3293–3295.
22. **Sirawaraporn, W., P. Prapunwattana, R. Sirawaraporn, Y. Yuthavong, and D. Santi.** 1993. The dihydrofolate reductase domain of *Plasmodium falciparum* thymidylate synthase-dihydrofolate reductase. J. Biol. Chem. **268:**21637–21644.
23. **Sirawaraporn, W., T. Sathitkul, R. Sirawaraporn, Y. Yuthavong, and D. Santi.** 1997. Antifolate-resistant mutants of *Plasmodium falciparum* dihydrofolate reductase. Proc. Natl. Acad. Sci. USA **94:**1124–1129.
24. **Taylor, P. C., F. D. Schoenknecht, J. C. Sherris, and E. C. Linner.** 1983. Determination of minimum bactericidal concentrations of oxacillin for *Staphylococcus aureus*: influence and significance of technical factors. Antimicrob. Agents Chemother. **23:**142–150.
25. **Trujillo, M., R. Donald, D. Roos, P. Greene, and D. Santi.** 1996. Heterologous expression and characterization of bifunctional dihydrofolate reductase-thymidylate synthase enzyme of *Toxoplasma gondii*. Biochemistry **35:**6366–6374.
26. **Visalli, M. A., M. R. Jacobs, and P. C. Appelbaum.** 1996. MIC and time-kill study of activities of DU-6859a, ciprofloxacin, levofloxacin, sparfloxacin, cefotaxime, imipenem, and vancomycin against nine penicillin-susceptible and -resistant pneumococci. Antimicrob. Agents Chemother. **40:**362–366.